Impact of susceptibility-induced distortion correction on perfusion imaging by pCASL with a segmented 3D GRASE readout

Catarina Domingos [a,b,*], Ana R. Fouto [a], Rita G. Nunes [a], Amparo Ruiz-Tagle [a], Inês Esteves [a], Nuno A. Silva [c], Pedro Vilela [d], Raquel Gil-Gouveia [d,e], Patrícia Figueiredo [a]

[a] Institute for Systems and Robotics - Lisboa and Department of Bioengineering, Instituto Superior Técnico, Universidade de Lisboa, Lisbon, Portugal
[b] Agência Regional para o Desenvolvimento da Investigação, Tecnologia e Inovação, Funchal, Portugal
[c] Learning Health, Hospital da Luz, Lisbon, Portugal
[d] Neurology Department, Hospital da Luz, Lisbon, Portugal.
[e] Center for Interdisciplinary Research in Health, Universidade Católica Portuguesa, Lisbon, Portugal

ARTICLE INFO

ABSTRACT

Purpose: The consensus for the clinical implementation of arterial spin labeling (ASL) perfusion imaging recommends a segmented 3D Gradient and Spin-Echo (GRASE) readout for optimal signal-to-noise-ratio (SNR). The correction of the associated susceptibility-induced geometric distortions has been shown to improve diagnostic precision, but its impact on ASL data has not been systematically assessed and it is not consistently part of pre-processing pipelines. Here, we investigate the effects of susceptibility-induced distortion correction on perfusion imaging by pseudo-continuous ASL (pCASL) with a segmented 3D GRASE readout.
Methods: Data acquired from 28 women using pCASL with 3D GRASE at 3T was analyzed using three pre-processing options: without distortion correction, with distortion correction, and with spatial smoothing (without distortion correction) matched to control for blurring effects induced by distortion correction. Maps of temporal SNR (tSNR) and relative perfusion were analyzed in eight regions-of-interest (ROIs) across the brain.
Results: Distortion correction significantly affected tSNR and relative perfusion across the brain. Increases in tSNR were like those produced by matched spatial smoothing in most ROIs, indicating that they were likely due to blurring effects. However, that was not the case in the frontal and temporal lobes, where we also found increased relative perfusion with distortion correction even compared with matched spatial smoothing. These effects were found in both controls and patients, with no interactions with the participant group.
Conclusion: Correction of susceptibility-induced distortions significantly impacts ASL perfusion imaging using a segmented 3D GRASE readout, and this step should therefore be considered in ASL pre-processing pipelines. This is of special importance in clinical studies, reporting perfusion across ROIs defined on relatively undistorted images and when conducting group analyses requiring the alignment of images across different subjects.

1. Introduction

Arterial spin labeling (ASL) is a Magnetic Resonance Imaging (MRI) technique that enables imaging brain perfusion non-invasively, by magnetically labeling arterial blood water protons to obtain an endogenous blood flow tracer [1]. Since it is completely non-invasive, ASL may provide a good alternative to conventional techniques such as dynamic susceptibility contrast (DSC) MRI that rely on the intravenous injection of a paramagnetic contrast agent [2]. Given its great potential

in various clinical applications [3], a consensus paper was published with recommendations for the clinical implementation of ASL perfusion imaging [4]. For optimal signal-to-noise ratio (SNR) of the intrinsically small perfusion-weighted signal given by the difference between control and label images, the current recommendation [4] is to combine pseudo-continuous ASL (pCASL) with background suppression (BS) and 3D readout schemes such as multi-echo stack-of-spirals 3D Rapid Imaging with Refocused Echoes (RARE) or 3D Gradient and Spin-Echo (GRASE). In fact, BS has been shown to improve temporal SNR (tSNR), while 3D

acquisition improves spatial SNR compared with 2D readouts [5].

Not only do 3D sequences provide higher SNR than multi-slice 2D sequences, but they also allow much more efficient BS, and in this way considerably enhance the ASL perfusion SNR [5]. However, single-shot 3D acquisitions may suffer from severe through-plane blurring and susceptibility induced geometric distortions, due to the inherently longer readout times with associated T2(*) weighting and increased sensitivity to B_0 field inhomogeneities. While blurring is a result of the widening of the point-spread function (PSF) with T2(*) decay, geometric distortions happen due to T2(*) weighting in the presence of field inhomogeneities. In general, blurring and geometric distortions can happen in both the through-plane and in-plane phase encoding directions. However, in sequences like 3D GRASE where refocusing is performed between planes, only T2 decay occurs along the slice direction and hence distortion happens mostly in the in-plane direction. On the other hand, the readout time is longer between planes, leading to greater blurring through-plane than in-plane. This is considerably reduced by using segmented 3D acquisitions, due to their shorter effective echo times and readout durations [6]. For this reason, segmented 3D sequences are recommended to achieve an appropriate balance between SNR, susceptibility effects and through-plane blurring. However, the number of segments used can affect the balance between these three factors and should be considered in the acquisition planning [7].

Although commonly implemented segmented 3D sequences such as 3D GRASE do not produce significant through-plane blurring, they may still exhibit considerable in-plane magnetic field inhomogeneities due to susceptibility effects [6]. These effects are typically observed at tissue/air or tissue/bone interfaces and they are characterized by geometric deformations with hyper/hypo intensities introduced along the phase encoding (PE) direction [8,9]. Besides impairing ASL data quality, such distortions may compromise analysis over regions-of-interest (ROIs) defined based on other (relatively undistorted) images or atlases, or group analyses requiring image alignment between subjects (with different distortions). In fact, one of the recommendations of the ASL consensus paper was that the description of the distortion correction methods should be provided to ensure an accurate comparison between different sites [4].

Several techniques have been developed to correct for susceptibility distortion artefacts induced by field inhomogeneities, including the commonly used FMRIB's Utility for Geometrically Unwarping echo-planar imaging (FUGUE) [10]; an algorithm proposed by Jezzard et al. [11] that uses a residual fieldmap to characterize field inhomogeneities; a tool for estimating and correcting susceptibility induced distortions (TOPUP) [12]; and deep learning methods such as a 2D neural network (U-net) [13]. The correction of susceptibility distortions is routinely performed in blood oxygenation level-dependent (BOLD) functional MRI (fMRI) studies [14], and it is essential in the pre-processing of diffusion MRI data, where distortions are additionally aggravated by eddy currents induced by the strong diffusion-weighting gradients [15]. In terms of ASL analysis tools, considering the ASL pipeline inventory list made available by the OSIPI Task Force 1.1 (https://osipi.org/task-force-1-1/), distortion correction is included as a pre-processing step in some (namely Bayesian Inference for Arterial Spin Labeling (BASIL) [16] MRI, Quantiphyse [17] and ExploreASL [18]), but not others (ASL-MRICloud [19] and ASLtoolbox [20]). Additionally, several studies reporting perfusion in different brain regions do not indicate distortion correction as part of their data analysis procedure [21–23]. Moreover, in pathology it is often desirable to assess perfusion in ROIs defined on relatively undistorted images (tissue ROIs as well as ROIs related with lesions, e.g., white matter hyperintensities, stroke, or tumor) [3,24,25].

To our knowledge, only two studies have evaluated the effect of distortion correction on ASL data [26,27] to date. Madai et al. [26] compared ASL with or without distortion correction with DSC, in terms of the relative perfusion measurements in the anterior, middle and posterior cerebral artery territories of patients with chronic steno-occlusive disease. They found that distortion correction improved diagnostic accuracy and made ASL more comparable to DSC, and recommended this step in ASL analysis pipelines. Gai et al. [27] proposed a modification of a non-segmented 3D echo planar imaging (EPI) readout to include alternating k-space coverage along phase encoding direction for alternating dynamic acquisitions of control and label pairs. Although their main goal was to show the benefit of their sequence modification in terms of distortion correction, they did observe an improved match between perfusion maps and corresponding non-distorted gray matter (GM) masks after distortion correction. Although both studies showed significant effects of distortion correction on ASL perfusion images, its impact on ASL data quality (in terms of the temporal SNR) and ensuing regional perfusion measurements was not systematically assessed, and the importance of this pre-processing step has yet to be clearly established [18]. Besides, neither of the studies completely followed the consensus recommendations, with one using a non-segmented 3D EPI rather than a segmented 3D GRASE readout, which is proposed to reduce susceptibility effects as previously stated.

Here, we systematically investigate the effects of susceptibility distortion correction on perfusion imaging by pCASL with a segmented 3D GRASE readout, in terms of tSNR as well as perfusion measurements across different brain regions.

2. Materials and methods

2.1. Image acquisition

A group of 28 women (31±8 years) were recruited in the scope of a study on migraine, including 11 patients with episodic menstrually-related migraine without aura and 17 healthy controls.

The study was approved by the Hospital da Luz *Commission of Ethics for Clinical Investigation*. This study was carried out in accordance with the Declaration of Helsinki and all subjects provided written informed consent.

Volunteers were studied on a 3T Siemens Vida MRI system (Siemens, Erlangen, Germany) using a 64-channel receive head RF coil. Perfusion imaging was performed using pCASL (TR/TE = 5600.00 /18.40 ms, labeling duration = 1800.00 ms, post-labeling delay = 1800.00 ms, BS (BS-normal: 2 BS pulses, implemented in Siemens software version XA20A), 4 repetitions, total acquisition time = 3.06 min) with a segmented 3D GRASE readout (4 segments, 32 nominal partitions in the slice-encoding direction (z-direction) with 12.5% oversampling with centric encoding scheme, field of view (FOV) = 240 × 240 × 128 mm^3, voxel size = 3.8 × 3.8 × 4.0 mm^3, bandwidth = 3256 Hz/px, echo spacing = 0.40 ms, turbo factor = 10, EPI factor = 31, in-plane PE direction = P–A, Generalized Autocalibrating Partial Parallel Acquisition (GRAPPA) acceleration factor 2), following the consensus paper recommendations [4]. A 3D gradient-echo fieldmap (TE1/TE2 = 4.92 / 7.38 ms, FOV = 220 × 220 × 192 mm^3, voxel size = 3.4 × 3.4 × 3.0 mm^3) and a T1-weighted structural image (3D magnetization-prepared rapid gradient echo (MPRAGE), TI = 900 ms, TR/TE = 2300.00 / 2.98 ms, FOV = 256 × 240 × 128 mm^3, voxel size = 1.00 mm isotropic) were also acquired. The study from which the data used in this paper was retrieved encompassed various acquisitions, with an overall duration of approximately one hour, including an average 40-min interval between the acquisition of the fieldmap and the ASL data.

2.2. Image analysis

Image analysis was performed using FSL (fsl.fmrib.ox.ac.uk) [28], particularly FSL's BASIL toolbox [16], and MATLAB in-house tools (www.mathworks.com). Motion correction was performed using FSL's MCFLIRT [29]. One of the middle ASL control images was used as a reference, also for registration (below). To ensure that data were not corrupted by motion artefacts, we computed the mean absolute displacement for each subject and considered unacceptable motion if

this exceeded 1.00 mm [30]. We found average mean displacements between 0.11 mm and 0.71 mm (mean 0.46 mm), and therefore no subject was excluded. Furthermore, visual inspection was performed to verify that no severe motion, susceptibility, labeling or vascular artefacts were present in each perfusion map [4,18].

After motion correction: three pre-processing options were considered: i) no distortion correction (*nocorr*); ii) distortion correction based on a fieldmap using FSL's PRELUDE&FUGUE [31] (*corr*); and iii) without distortion correction but considering different degrees of spatial smoothing to control for potential effects of blurring induced by distortion correction (*smooth*) [32]. Spatial smoothing was performed using a 1D Gaussian filter along the in-plane PE direction, with different values of full width at half maximum (FWHM) [33], from 2.4 to 5.9 mm in steps of 0.2 mm, following the procedure employed by Renval et al. [33] The pre-processing pipeline is displayed in Fig. 1.

For each subject and pre-processing pipeline, pairwise subtraction of control and label images was performed to yield a time series of control-label subtraction images. The temporal mean (tMean) and the temporal standard deviation (tSD) were calculated voxelwise, and tSNR maps were obtained by dividing the tMean by tSD in each voxel. Perfusion maps were obtained by averaging the control-label subtraction images in the following conditions: i) without spatial regularization (*noreg*); ii) with spatial regularization using FSL's BASIL (*reg*) [34]; and iii) with spatial regularization and partial volume correction using FSL's BASIL (*regpvc*) [35].

The T1-weighted structural image was segmented using FSL's FAST [36] to obtain GM and white matter (WM) masks by thresholding the respective partial volume estimates (PVE) at 70% [23] and 90%, respectively. Furthermore, FSL's FIRST [37] was used to segment subcortical GM and brainstem regions. The T1-weighted structural image of each subject was co-registered with the Montreal Neurological Institute (MNI) standard space using FSL's tool FNIRT [38]. In total, the following eight anatomical ROIs were defined: frontal, temporal, parietal and occipital cortical GM, subcortical GM, cerebellum, brainstem, and WM (see Supplementary Material: Supporting Fig. S1). The four cortical GM and the cerebellum ROIs were obtained by the intersection of each subject's GM mask with regions defined in FSL's MNI structural atlas [39] (atlas probability >10%).

Registration was performed between the relatively distortion-free T1-weighted structural images and the pre-processed ASL images (without and with distortion correction), by using FSL's tool FLIRT [29] to estimate a linear (affine) registration with 12 degrees of freedom. The estimated registration transformations were then applied to transform the ROI images into the ASL space (without and with distortion correction). For each ROI, the average tSD, tSNR and relative perfusion values were obtained, for each of the three pre-processing options (*nocorr, corr, smooth*) and the three perfusion mapping methods (*noreg, reg, regpvc*) (in the case of perfusion).

To illustrate the effects of distortion correction on the image geometry, the overlap between a GM mask obtained from the relatively undistorted T1-weighted structural image (Structural GM) and a GM mask obtained based on the ASL perfusion map (Perfusion GM) (with or without distortion correction) was evaluated. The Structural GM mask was defined by including the cortical GM, brainstem, cerebellum, and subcortical masks, obtained from the segmentation of the T1-weighted structural image. The Perfusion GM mask was defined by thresholding the ASL perfusion map to exclude WM [27] (the threshold value was manually determined for each subject). After registration of the Structural GM (using FSL's tool FLIRT [29]) to the ASL space of each subject (with or without distortion correction), we quantified the geometric
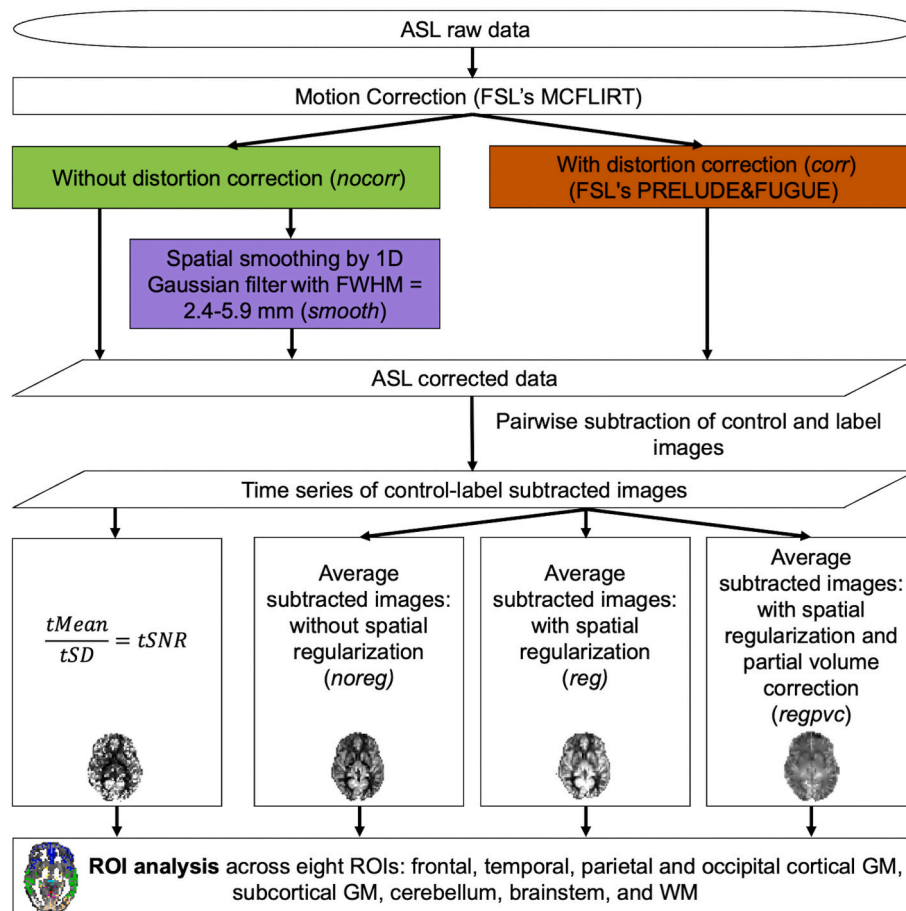

Fig. 1. Representation of the pre-processing pipeline followed in this study.

distortion effects by computing the number of voxels belonging to the intersection between the Structural and Perfusion GM masks (the matching voxels) in each case (with and without distortion correction), and then obtained the percent difference between them. A paired *t*-test was applied to test whether this difference was significant across subjects.

2.3. Statistical analysis

Statistical analysis was carried out using JASP 0.14.1 (jasp-stats.org). We analyzed the results for tSNR and perfusion (*noreg, reg, regpvc*) using a three-way repeated-measures analysis of variance (ANOVA) to test for effects of within-subjects' factors: ROI, Correction (*nocorr, corr, smooth*) and Group (*controls, patients*). For statistically significant main effects and interactions ($P < 0.05$), post-hoc *t*-tests were performed with Bonferroni correction for multiple comparisons.

3. Results

3.1. Effects on geometric distortions

The effects of susceptibility distortion correction on the perfusion images are illustrated in Fig. 2. Distortion correction improved the alignment between the structural GM borders and the underlying gray-to-white matter border in the perfusion image (as indicated by the arrows). Consistently with this visual appreciation, we also found that the number of mismatching voxels between the GM masks obtained from the two images decreased with distortion correction (number of blue voxels in the right images). A *t*-test showed a significant increase in the number of matching voxels between the T1- and perfusion-based GM

masks when performing distortion correction (median of 0.8% across subjects, $P < 0.001$). Overall, Fig. 2 indicates that distortion correction improved the alignment between the perfusion image and the relatively undistorted structural image. Geometric distortions are more evident in the frontal and inferior temporal lobes, and brainstem, in the majority of the subjects (21 out of 28), which is consistent with the greater sensitivity to susceptibility effects caused by nearby air-tissue interfaces in these regions.

The effects of distortion correction on the perfusion-weighted images are illustrated in Fig. 3, compared with no distortion correction as well as with the different levels of spatial smoothing tested. By subtracting the images with no distortion correction from the one with distortion correction, we can clearly observe changes across the brain, which are mostly located in the frontal lobe. Interestingly, although specific smoothing levels were found to match the effects of distortion correction in terms of tSD in specific brain regions (next section), we can see in Fig. 3 that none of them yields perfusion images that are more similar to the distortion-corrected image than the one without smoothing. Indeed, increasing smoothing levels are found to produce mostly increased loss of detail (tissue border / high frequencies) in the images.

Based on Figs. 2 and 3, we may conclude that distortion correction was effective in better aligning perfusion images with relatively undistorted structural images, while spatial smoothing did not produce similar effects to distortion correction.

3.2. Effects on temporal SD

Fig. 4 shows the results of tSD of the ASL control-label time series data in each ROI compared between distortion correction and different levels of spatial smoothing. The smoothing FWHM level that yielded the
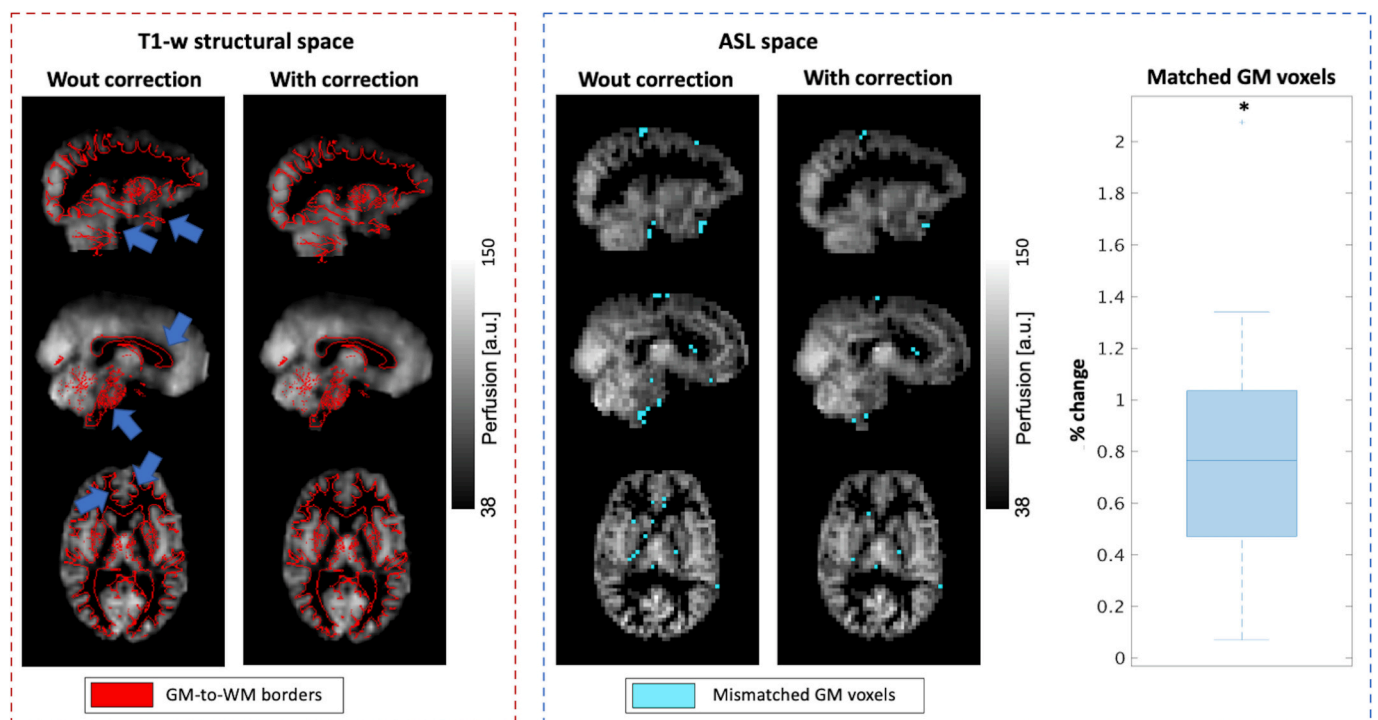

Fig. 2. Matching between the GM masks obtained from the relatively undistorted T1-weighted structural image (Structural GM) and the ASL perfusion image (Perfusion GM), without and with distortion correction: illustration for three representative slices of an illustrative subject and group results. Left: Thresholded perfusion images (Perfusion GM) registered to the structural space, with the gray-to-white matter (GM-to-WM) borders of the Structural GM overlaid (in red); the arrows highlight regions where distortion correction improved the alignment between the two GM masks. Middle: Thresholded perfusion images (Perfusion GM) in their native space, overlaid on top of the Structural GM mask (in blue); only mismatching voxels (belonging to the Structural GM mask but not the Perfusion GM) are visible. Right: The boxplot shows the distribution across subjects of the percent increase with distortion correction in the number of matching voxels between the Structural and Perfusion GM masks. * indicates a significant increase ($P < 0.001$). (For interpretation of the references to colour in this figure legend, the reader is referred to the web version of this article.)
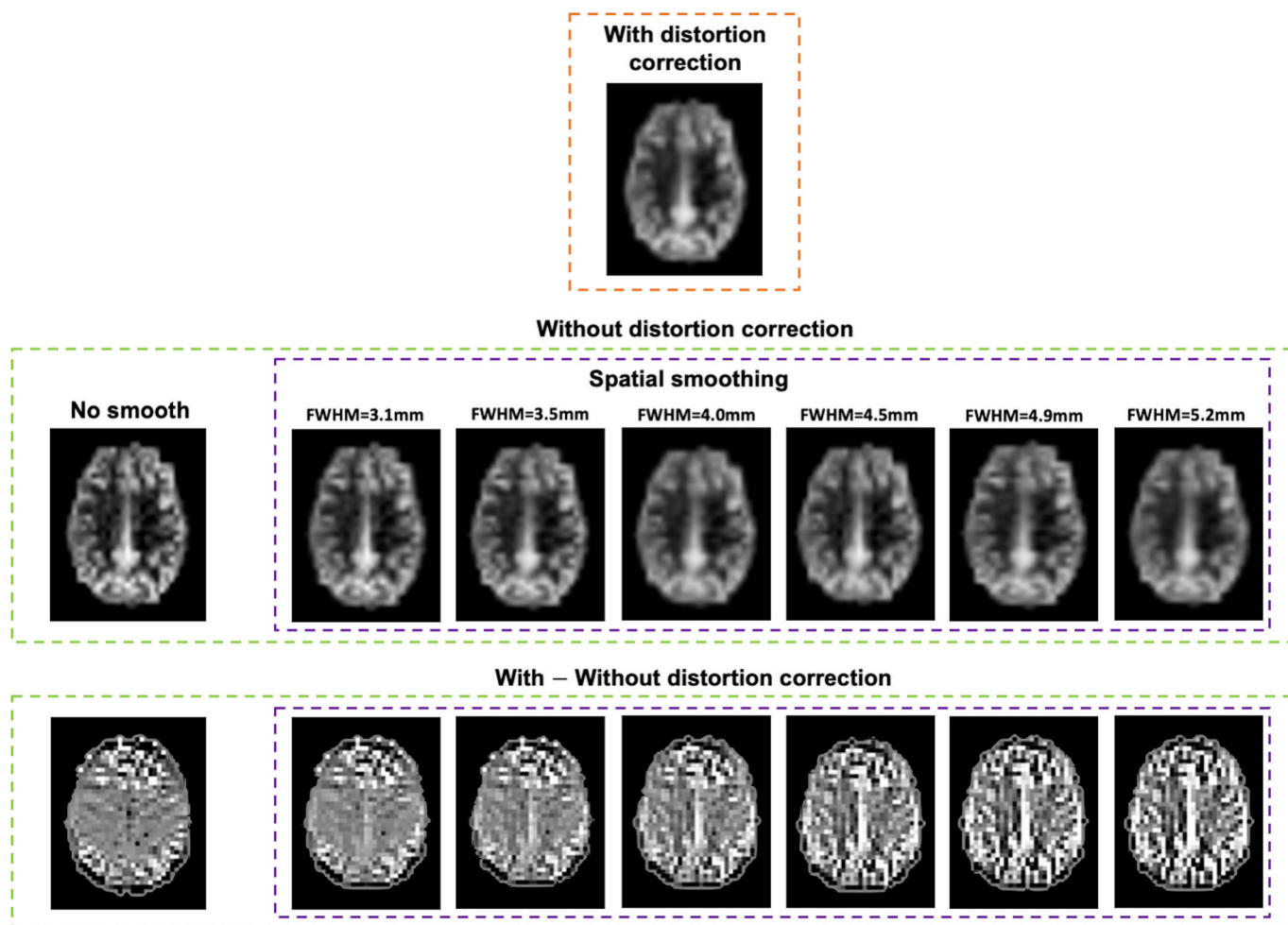
Fig. 3. Effects of distortion correction and spatial smoothing on perfusion-weighted images: example for one representative slice of one illustrative subject. The image obtained with distortion correction (top row, orange box) is compared with the images without distortion correction below (middle row): with no smoothing (left, green box), and with different degrees of spatial smoothing (right, purple box). To emphasize differences, the subtraction images between the image with distortion correction (top row) and each of the images without correction (middle row) are also shown below (bottom row). (For interpretation of the references to colour in this figure legend, the reader is referred to the web version of this article.)

median tSD value closest to the one of the respective distortion corrected data, for each ROI, is highlighted. This varies across ROIs, consistently with the impact of susceptibility artefacts. For example, in the brainstem, an area more affected by B_0 inhomogeneities, a higher FWHM was found.

3.3. Effects on temporal SNR

The values obtained for tSD and tSNR using the three pre-processing pipelines (*nocorr, corr, smooth*) were then compared, as presented in Fig. 5. Although for the tSNR analyzes only the level of FWHM that matched with the tSD of the distortion correction was considered, the variations of the tSNR with the level of smoothness can also be found in Fig. S2 in the Supplementary Material.

Three-way repeated measures ANOVA showed a significant main effect of ROI and Correction, as well as a significant interaction between them, with no effects of Group, for both tSD and tSNR.

Post-hoc tests revealed a significant tSD decrease when performing distortion correction, for all ROIs except the parietal area. As expected, this significant decrease was also observed when performing spatial smoothing, with no significant differences between distortion correction and spatial smoothing.

In contrast, significant differences in tSNR were found when performing distortion correction, even compared with spatial smoothing, in

the frontal and temporal ROIs, with an average change of $10.2\pm3.5\%$ and $8.4\pm2.4\%$, respectively, between with and without distortion correction. This is consistent with the greater susceptibility effects in these regions.

3.4. Effects on perfusion

The group results for the mean relative perfusion values obtained with the three perfusion estimation methods (*noreg, reg, regpvc*), using the three pre-processing pipelines (*nocorr, corr, smooth*), in each ROI, are presented in Fig. 6. For comparison with the *smooth* pipeline, the matched FWHM was selected based on the tSD results. However, perfusion variations (*noreg*) with the level of smoothing can also be found in Fig. S3 and Table S1 of the Supplementary Material, showing the ROI average perfusion values obtained with the three pre-processing pipelines.

Significant main effects of Correction and ROI were found for perfusion obtained with all estimation methods, with significant interactions between them and with no effects of Group.

When compared to no correction, spatial smoothing produced small but significant changes in perfusion (average change of $1.9\pm0.7\%$) in all ROIs except subcortical GM, for all estimation methods. Specifically, smoothing decreased perfusion in the cortical GM and brainstem ROIs and increased perfusion in the WM ROI: these effects are consistent with
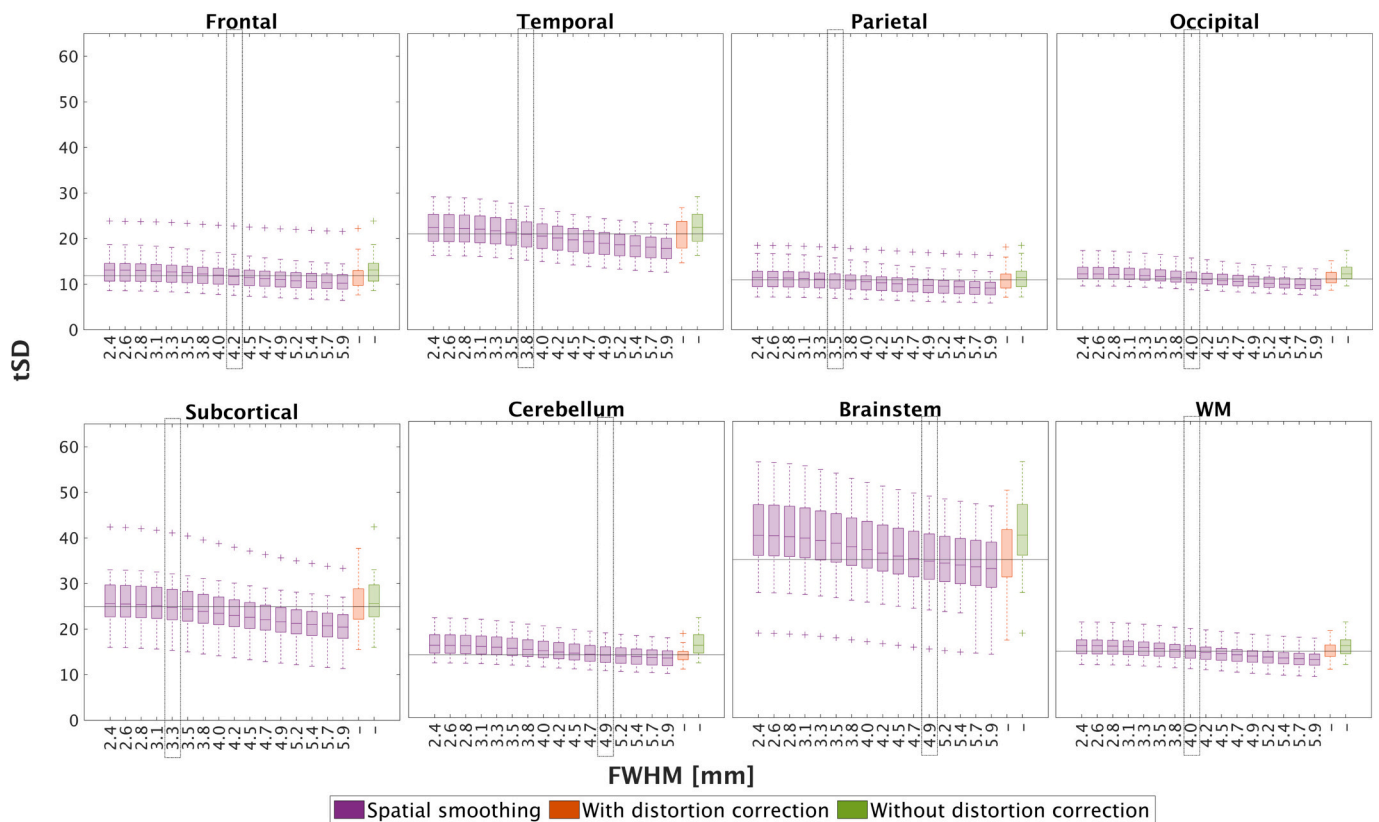
Fig. 4. Temporal standard deviation (tSD) in eight ROIs, obtained with and without distortion correction (right) and with different degrees of spatial smoothing (left, FWHM). Boxplots represent distributions across subjects, for ASL data without distortion correction (green), with spatial smoothing (purple), and with distortion correction (orange). The black box identifies the value of FWHM that matches the tSD obtained for distortion correction, in each ROI. This varies across ROIs, consistently with the impact of susceptibility artefacts. For example in the brainstem, an area more affected by B_0 inhomogeneities, a higher FWHM was found. The horizontal lines indicate the median of the values with distortion correction. (For interpretation of the references to colour in this figure legend, the reader is referred to the web version of this article.)

the partial volume effects between GM and WM resulting from smoothing across the borders between tissues.

When comparing distortion correction with no correction, the only significant perfusion changes that could not be explained by spatial smoothing were increases in the subcortical GM (average change of $1.0\pm0.9\%$) and the temporal cortex (only with spatial regularization with an average change of $1.3\pm1.7\%$), if not performing partial volume correction. Significantly decreased perfusion was also found in the occipital cortex and the cerebellum for all estimation methods; however, these decreases could be explained by spatial smoothing (since they were already present with spatial smoothing, and no significant differences were found between this and distortion correction).

4. Discussion

The results obtained show that distortion correction has an impact on ASL data analysis, not only increasing the tSNR but also significantly affecting perfusion values in various brain regions.

4.1. Effects on geometric distortions

The image geometric distortions produced by the susceptibility effects associated with the segmented 3D GRASE readout used in our study were more evident in the frontal and inferior temporal lobe, brainstem, caudate and putamen (subcortical ROI) regions. This is consistent with the study by Vidorreta et al. [6], reporting distortions in orbito-frontal regions and signal loss in inferior–temporal lobe regions when using a similar sequence. Other studies using a 3D GRASE sequence, also reported geometric distortions in the frontal sinus [27,40]. Using an EPI

sequence, susceptibility artefacts are present in similar regions (frontal and temporal lobes and ventricles) even more pronouncedly, as expected since EPI is more susceptible to these distortions than 3D GRASE [26,41].

4.2. Effects on temporal SNR

We observed a systematic and significant increase in tSNR, when performing distortion correction across all brain regions. This increase was found in each individual subject, and not only on average. This is consistent with previous reports [32,42], and may be at least partly associated with spatial blurring induced by the correction algorithm. Indeed, this hypothesis was corroborated by a consistent reduction in tSD with distortion correction. To clarify to what extent tSD reductions and tSNR increases could be explained by blurring effects, we followed the approach suggested by Renvall et al. [33] and generated ASL data without distortion correction but with spatial smoothing.

We found that indeed it was possible to find a specific level of spatial smoothing that produced decreases in tSD that were not significantly different from those produced by distortion correction. Consistently with the interpretation of blurring induced by distortion correction, we found that the level of spatial smoothing required to produce matching tSD decreases varied across brain regions in agreement with the spatial heterogeneity of susceptibility effects, i.e., with larger values found in more affected regions such as the frontal lobe or the brainstem. Although the tSNR values increases could also be explained by spatial smoothing in some regions, that was not the case in the frontal and temporal lobes. The distinct alterations in these regions could be related with the fact that they are more affected by geometric distortions and
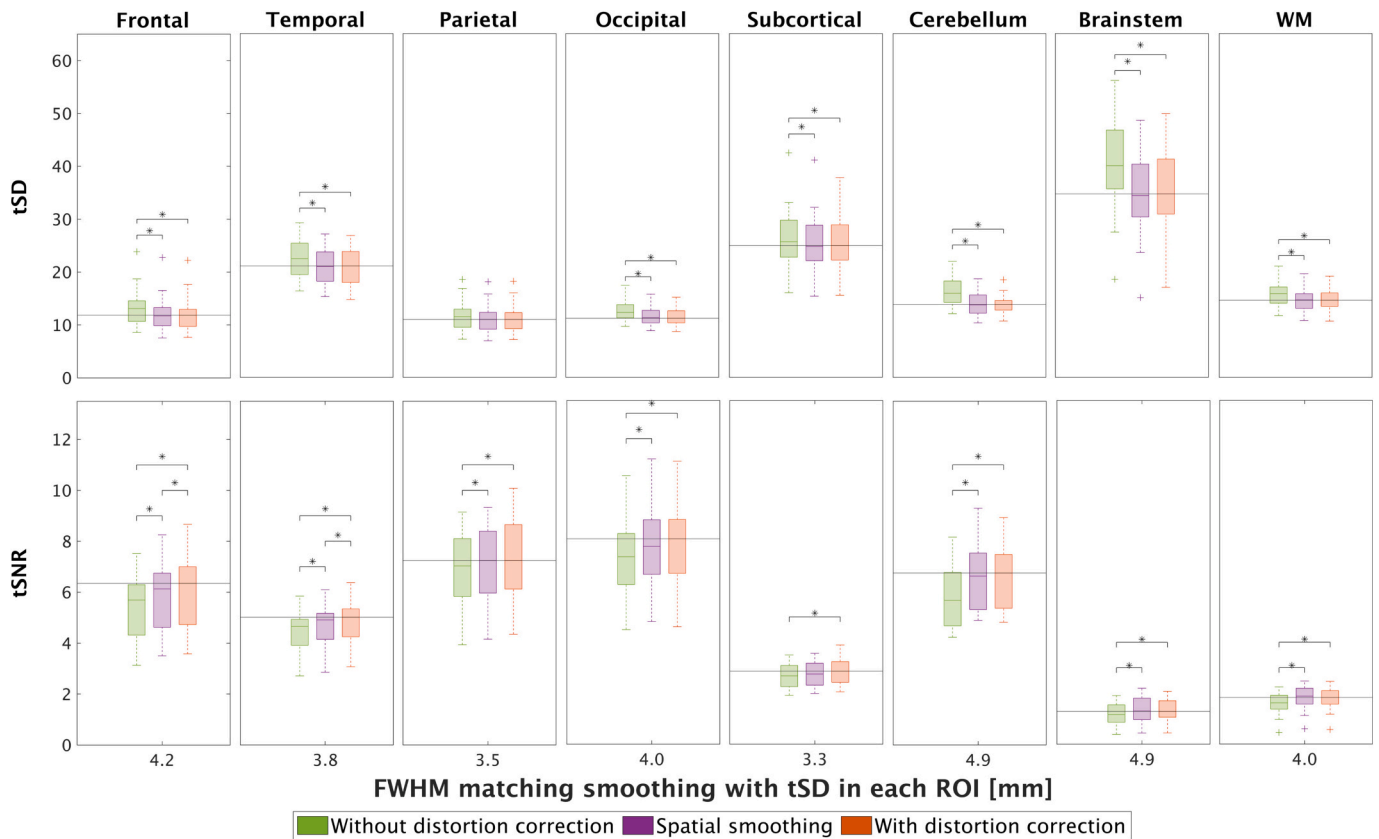
Fig. 5. Temporal standard deviation (tSD, top) and temporal SNR (tSNR, bottom) in eight ROIs, obtained with and without distortion correction and with matching spatial smoothing (FWHM). Boxplots represent distributions across subjects, for ASL data without distortion correction (green), with spatial smoothing (purple), and with distortion correction (orange). Three-way repeated measures ANOVA showed a significant main effect for ROI and Correction, as well as a significant interaction between them. The asterisk indicates significant differences obtained by post-hoc tests, corrected for multiple comparisons The horizontal lines indicate the median of the values with distortion correction. (For interpretation of the references to colour in this figure legend, the reader is referred to the web version of this article.)

hence more prone to effects of distortion correction.

4.3. Effects on perfusion

Having found that distortion correction led to increases of tSNR in some brain regions that were not fully explained by reductions in tSD induced by the associated blurring, we hypothesized that these would reflect increases in the measured perfusion values in those regions. Indeed, we found increases of perfusion in the temporal lobe and the subcortical GM that could not be explained by spatial smoothing. Although they were not significant, small increases were also found in the frontal lobe. Not only could spatial smoothing not explain such increases, but in fact it produced decreases instead. These alterations could be explained by the voxels shifting between ROIs upon registration.

Spatial regularization is often applied in the estimation of the perfusion image; it involves the application of an adaptive spatial smoothing prior to the data that effectively reduces the appearance of noise in the final perfusion map [34]. Given the effects of blurring associated with distortion correction, we sought to analyze how this could interact with spatial regularization. In general, the effects of spatial smoothing and distortion correction on the ROI perfusion values did not differ between applying spatial regularization or not.

Another option in the estimation of perfusion maps that could interact with the effects of distortion correction is the correction for partial volume effects. This aims to estimate the contributions of perfusion to the ASL signal separately for GM and WM in every voxel, based on each tissue's volume fraction within the voxel obtained from the segmentation of a structural image. This estimation is based on a

local linear regression, that quantifies the proportion of GM and WM in each voxel. Because there is no coherent ASL difference signal arising from cerebrospinal fluid (CSF), the CSF magnetization variation is considered to be zero and is not taken into account [35]. The variations with partial volume correction were similar to those previously reported [23], in particular showing a large perfusion increase in the subcortical GM. Probably as a consequence of this effect, the perfusion increase produced by distortion correction in this region was no longer observed with this estimation method. Nonetheless, it is recommended to always present results both with and without partial volume correction [43].

4.4. Relation with the literature

Only two studies have previously investigated the effects of susceptibility distortion correction on ASL perfusion measurements [26,27]. The former showed that performing correction improved diagnostic accuracy in steno-occlusive disease, and that the relative perfusion measurements in large arterial territories were more similar to those obtained with DSC. However, the extent to which these changes may be attributed to the increased tSNR produced by the associated blurring were not investigated. Our study provides a detailed analysis of these effects, showing that perfusion changes observed across the brain are indeed partly explained by spatial smoothing. By combining our findings with the ones by Madai et al. [26], we may conclude that distortion correction significantly changes perfusion values across the brain, and may improve diagnostic accuracy when compared with conventional techniques.

Moreover, although the results of Madai et al. [26] strongly support the use of distortion correction in ASL data analysis, they only pertain to
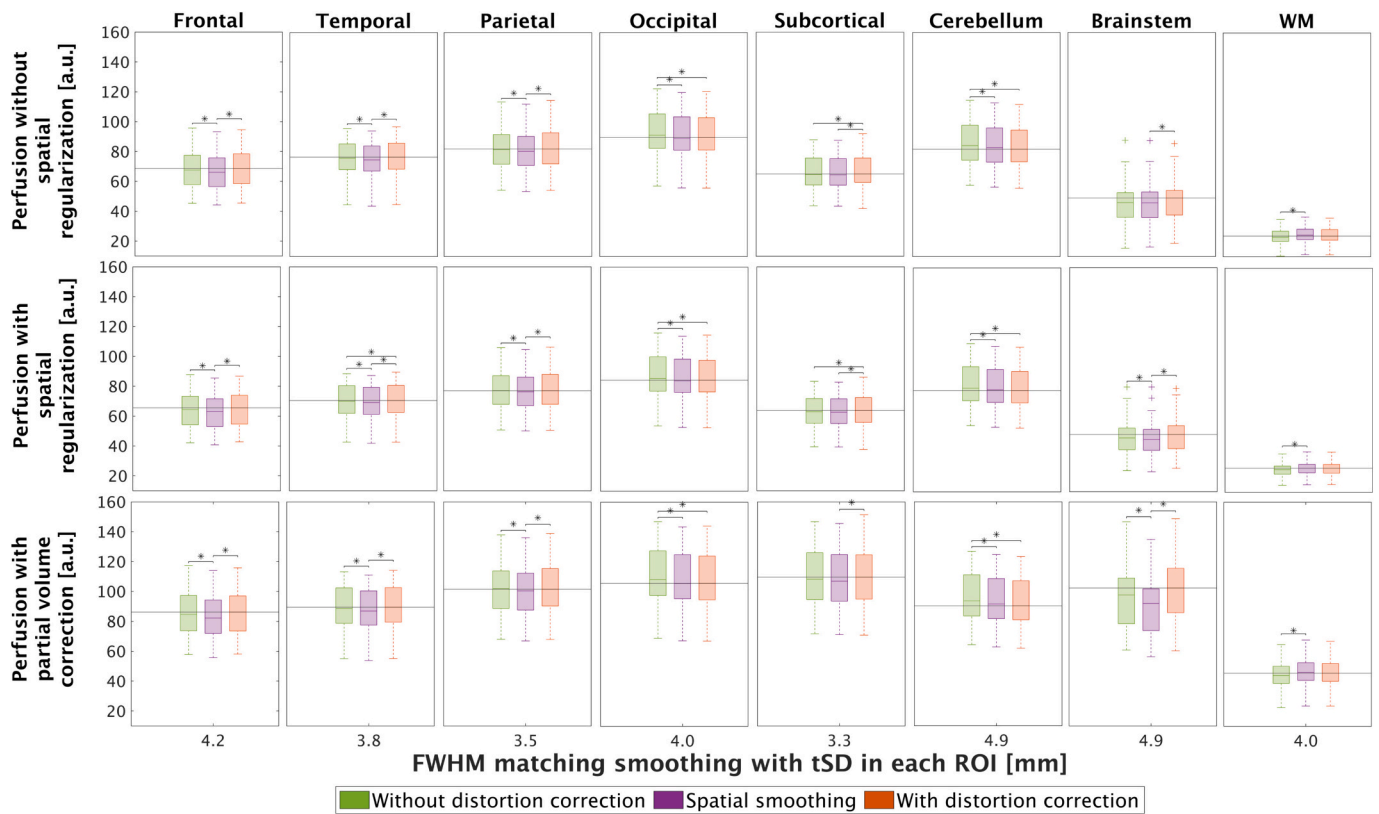
Fig. 6. Perfusion relative values in eight ROIs, obtained with and without distortion correction and with matching spatial smoothing (FWHM), for different perfusion estimation methods: without spatial regularization (top), with spatial regularization (middle), and with spatial regularization and partial volume correction (bottom). Boxplots represent distributions across subjects, for ASL data without distortion correction (green), with spatial smoothing using matched FWHM (purple) and with distortion correction (orange). Three-way repeated measures ANOVA showed a significant main effect for ROI and Correction, as well as a significant interaction between them. The asterisk indicates significant changes obtained by post-hoc tests, corrected for multiple comparisons. The horizontal lines indicate the median of the values with distortion correction. (For interpretation of the references to colour in this figure legend, the reader is referred to the web version of this article.)

perfusion averaged across large brain regions and therefore cannot be directly compared with our results nor can they be more generally extrapolated to studies analyzing perfusion across multiple ROIs. Also, the sequence used in this study differed from the consensus recommendations (PASL rather than pCASL, and multi-delay rather than single-delay); however, these differences should not affect the results considerably.

4.5. Limitations

Here we employed an ASL acquisition using the recommended segmented 3D GRASE readout for clinical applications. The susceptibility distortions and their impact on perfusion measurements would certainly vary when using different readout schemes. Therefore, our results cannot be directly generalizable to studies employing different readout schemes. They can, however, be generalized to other studies using the same sequence, which is the sequence recommended by the consensus paper and the product sequence implemented on the main MRI systems, and therefore the most used in clinical studies. Nevertheless, it is important to note that studies investigating pathologies such as stroke or concussion may yield different results due to the typical characteristics of hemorrhage associated with these types of pathologies, which may disturb the field and increase susceptibility distortions [44]. Studies at higher field strengths will also suffer from increased susceptibility artefacts, and the effects of distortion correction would have to be evaluated specifically [45].

To perform distortion correction, we used the FUGUE tool from FSL which performs a fieldmap-based correction. However, other distortion corrections methods could be used, such as TOPUP, which is based on

images with opposite PE directions [12]. In the presence of large amounts of motion, using a method that corrects for the PE and the reserved direction, or incorporating dynamic distortion correction techniques [31], can be advantageous, because geometric distortions may no longer correspond to the original direction due to inter-scan in plane rotations. Previous studies have indicated that the effectiveness of distortion correction is similar when utilizing either a fieldmap (e.g., using FSL's FUGUE tool) or TOPUP [13]. Consequently, FUGUE can be considered as an appropriate alternative in cases where the acquisition of images with opposite PE direction is not possible, as was the case of our study. With BASIL [16] and Quantiphyse ASL [17] analysis tools, it is possible to perform the correction using either of the two methods (FUGUE or TOPUP), although Explore ASL [18] only has TOPUP implemented.

The relatively long time difference between the ASL and fieldmap acquisitions may impact the effectiveness of the distortion correction results due to potential instability in the fieldmap, for example as a result of head motion. The most prominent distortions were corrected in our data, as assessed by the improved alignment with the relatively distortion-free structural images, suggesting that the fieldmap was sufficiently stable during the study. Nevertheless, we further assessed the stability of the fieldmap indirectly, by comparing the geometric distortions in our ASL data with those observed in a functional MRI dataset with a 2D EPI readout recorded immediately after the fieldmap (results not shown). A simple visual comparison showed generally similar distortions in both datasets. Furthermore, we also registered the fMRI and ASL datasets with each other using linear rigid body transformations, after distortion correction, and found good alignment. Overall, these findings suggest that, in your dataset, the geometric distortions were

sufficiently stable for an effective correction.

We did not acquire a calibration image and perfusion images were therefore obtained only in arbitrary units (relative perfusion). To obtain quantitative perfusion images in absolute units of perfusion, ml/100 g/min, the relative perfusion maps should be normalized by the equilibrium magnetization of the arterial blood (M_{0a}) which can be estimated based on a proton density image acquired with a similar readout to the ASL data to obtain a map of M_{0t} – the calibration image [46]. Two options may be considered to estimate M_{0a} from M_{0t}: a voxelwise approach to estimate M_{0a} in each voxel, or an ROI approach to estimate a single M_{0a} value from the average M_{0t} value in a specific brain compartment [46]. In the ROI approach, a region within the lateral ventricles is usually chosen because it can be robustly defined with minimal partial volume effects and geometric distortions. In this case, distortions of the calibration image are therefore not expected to affect the M_{0a} value. If a voxelwise approach is chosen, then the proton density image would be affected by the same susceptibility effects suffered by the ASL image [46], However, this image usually undergoes spatial smoothing before conversion into M_{0a}, which should minimize the impact of those effects on the final calibrated perfusion image. For these reasons, we believe that our results regarding the effects of distortion correction on the relative perfusion images should be largely applicable to calibrated perfusion images as well.

Registration between the ASL and structural spaces is usually performed based on a proton density image. In our study, since this was not acquired, we performed registration using an ASL control image instead. Although the tissue contrast of the image is reduced relative to a proton density image, it was nevertheless sufficient to obtain an accurate registration to the T1-weighted structural image of the subject.

5. Conclusion

To conclude, we demonstrated that susceptibility distortion correction has a significant impact on ASL perfusion measurements using a segmented 3D GRASE readout in several brain regions, which cannot be fully explained by the associated blurring effects. Our findings contribute to the ASL perfusion imaging literature, by helping clarify the often-neglected step of susceptibility distortion correction in the pre-processing pipeline. This is of special importance when considering clinical applications where protocol and data harmonization are most critical.

CRediT authorship contribution statement

Catarina Domingos: Conceptualization, Methodology, Formal analysis, Software, Writing – original draft, Writing – review & editing. **Ana R. Fouto:** Data curation, Investigation, Writing – review & editing. **Rita G. Nunes:** Investigation, Methodology, Writing – review & editing. **Amparo Ruiz-Tagle:** Data curation, Investigation. **Inês Esteves:** Data curation, Investigation. **Nuno A. Silva:** Investigation. **Pedro Vilela:** Investigation. **Raquel Gil-Gouveia:** Investigation. **Patrícia Figueiredo:** Conceptualization, Methodology, Writing – original draft, Writing – review & editing, Supervision, Project administration, Funding acquisition.

Declaration of Competing Interest

There is no conflict of interest to declare.

Acknowledgments

Appendix A. Supplementary data

Supplementary data to this article can be found online at https://doi.org/10.1016/j.mri.2023.06.010.

References

[1] Williams DS, Detre JA, Leigh JS, Koretsky AP. Magentic resonance imaging of perfusion using spin inversion of arterial water. Proc Natl Acad Sci U S A 1992;89 (1):212–6. https://doi.org/10.1073/pnas.89.1.212.

[2] Haller S, Zaharchuk G, Thomas DL, Lovblad KO, Barkhof F, Golay X. Arterial spin labeling perfusion of the brain: emerging clinical applications. Radiology. 2016; 281(2):337–56. https://doi.org/10.1148/radiol.2016150789.

[3] Bambach S, Smith M, Morris PP, Campeau NG, Ho M. Arterial spin labeling applications in pediatric and adult neurologic disorders 2022;55:698–719. https://doi.org/10.1002/jmri.27438.

[4] Alsop DC, Detre JA, Golay X, et al. Recommended implementation of arterial spin-labeled perfusion MRI for clinical applications: a consensus of the ISMRM perfusion study group and the European consortium for ASL in dementia. Magn Reson Med 2015;73(1):102–16. https://doi.org/10.1002/mrm.25197.

[5] Vidorreta M, Wang Z, Rodríguez I, Pastor MA, Detre JA, Fernández-Seara MA. Comparison of 2D and 3D single-shot ASL perfusion fMRI sequences. NeuroImage. 2013;66:662–71. https://doi.org/10.1016/j.neuroimage.2012.10.087.

[6] Vidorreta M, Balteau E, Wang Z, et al. Evaluation of segmented 3D acquisition schemes for whole-brain high-resolution arterial spin labeling at 3 T. NMR Biomed 2014;27(11):1387–96. https://doi.org/10.1002/nbm.3201.

[7] Paschoal AM, Leoni RF, Pastorello BF, van Osch MJP. Three-dimensional gradient and spin-echo readout for time-encoded pseudo-continuous arterial spin labeling: influence of segmentation factor and flow compensation. Magn Reson Med 2021;86 (3):1454–62. https://doi.org/10.1002/mrm.28807.

[8] Schallmo MP, Weldon KB, Burton PC, Sponheim SR, Olman CA. Assessing methods for geometric distortion compensation in 7T gradient echo functional MRI data. Hum Brain Mapp 2021;42(13):4205–23. https://doi.org/10.1002/hbm.25540.

[9] Graham MS, Drobnjak I, Jenkinson M, Zhang H. Quantitative assessment of the susceptibility artefact and its interaction with motion in diffusion MRI. PloS One 2017;12(10). https://doi.org/10.1371/journal.pone.0185647.

[10] Smith SM, Jenkinson M, Woolrich MW, et al. Advances in functional and structural MR image analysis and implementation as FSL. NeuroImage. 2004;23(S1): S208–19. https://doi.org/10.1016/j.neuroimage.2004.07.051.

[11] Jezzard P, Balaban RS. Correction for geometric distortion in echo planar images from B0 field variations. Magn Reson Med 1995;34(1):65–73. https://doi.org/10.1002/mrm.1910340111.

[12] Andersson JL, Skare S, Ashburner J. How to correct susceptibility distortions in spin-echo echo-planar images: application to diffusion tensor imaging. NeuroImage. 2003;20(2):870–88. https://doi.org/10.1016/S1053-8119(03)00336-7.

[13] Hu Z, Wang Y, Zhang Z, et al. Distortion correction of single-shot EPI enabled by deep-learning. Neuroimage. 2020;221:117170. https://doi.org/10.1016/j.neuroimage.2020.117170.

[14] Caballero-Gaudes C, Reynolds RC. Methods for cleaning the BOLD fMRI signal. NeuroImage. 2017;154:128–49. https://doi.org/10.1016/j.neuroimage.2016.12.018.

[15] Jezzard P, Barnett AS, Pierpaoli C. Characterization of and correction for eddy current artifacts in echo planar diffusion imaging. Magn Reson Med 1998;39: 801–12. https://doi.org/10.1002/mrm.1910390518.

[16] Chappell MA, Groves AR, Whitcher B, Woolrich MW. Variational Bayesian inference for a non-linear forward model. IEEE Trans Signal Process 2009;57(1): 223–36. https://doi.org/10.1109/TSP.2008.2005752.

[17] University of Oxford. Quantiphyse - Quantiphyse Documentation. Accessed June 30, 2022, https://quantiphyse.readthedocs.io/en/latest/asl/asl_tutorial.html; 2019.

[18] Mutsaerts HJMM, Petr J, Groot P, et al. ExploreASL: An image processing pipeline for multi-center ASL perfusion MRI studies. NeuroImage. 2020;219:117031. https://doi.org/10.1016/j.neuroimage.2020.117031.

[19] Li Y, Liu P, Li Y, et al. ASL-MRICloud: an online tool for the processing of ASL MRI data. NMR Biomed 2019;32(2):e4051. https://doi.org/10.1002/nbm.4051.

[20] Wang Z, Aguirre GK, Rao H, et al. Empirical optimization of ASL data analysis using an ASL data processing toolbox: ASLtbx. Magn Reson Imaging 2008;26(2): 261–9. https://doi.org/10.1016/j.mri.2007.07.003.

[21] Chen JJ, Rosas HD, Salat DH. Age-associated reductions in cerebral blood flow are independent from regional atrophy. Neuroimage. 2011;55(2):468–78. https://doi.org/10.1016/j.neuroimage.2010.12.032.

[22] Zhang N, Gordon ML, Ma Y, et al. The age-related perfusion pattern measured with arterial spin labeling MRI in healthy subjects. Front Aging Neurosci 2018;10:214. https://doi.org/10.3389/fnagi.2018.00214.

[23] Warnert EAH, Steketee RME, Vernooij MW, et al. Implementation and validation of ASL perfusion measurements for population imaging. Magn Reson Med 2020;84 (4):2048–54. https://doi.org/10.1002/mrm.28271.

[24] Dolui S, Tisdall D, Vidorreta M, et al. Characterizing a perfusion-based periventricular small vessel region of interest. NeuroImage Clin 2019;23:101897. https://doi.org/10.1016/j.nicl.2019.101897.

[25] Harston GW, Okell TW, Sheerin F, et al. Quantification of serial cerebral blood flow in acute stroke using arterial spin labeling. Stroke. 2017;48(1):123–30. https://doi.org/10.1161/STROKEAHA.116.014707.

[26] Madai VI, Martin SZ, von Samson-Himmelstjerna FC, et al. Correction for susceptibility distortions increases the performance of arterial spin labeling in patients with cerebrovascular disease. J Neuroimaging 2016;26(4):436–44. https://doi.org/10.1111/jon.12331.

[27] Gai ND, Chou YY, Pham D, Butman JA. Reduced distortion artifact whole brain CBF mapping using blip-reversed non-segmented 3D echo planar imaging with pseudo-continuous arterial spin labeling. Magn Reson Imaging 2017;44:119–24. https://doi.org/10.1016/j.mri.2017.08.011.

[28] Jenkinson M, Beckmann CF, Behrens TE, Woolrich MW, Smith SM. FSL. NeuroImage 2012;62(2):782–90. https://doi.org/10.1016/j.neuroimage.2011.09.015.

[29] Jenkinson M, Bannister P, Brady M, Smith S. Improved optimization for the robust and accurate linear registration and motion correction of brain images. NeuroImage. 2002;17(2):825–41. https://doi.org/10.1016/s1053-8119(02)91132-8.

[30] Leoni RF, Oliveira IA, Pontes-Neto OM, Santos AC, Leite JP. Cerebral blood flow and vasoreactivity in aging: an arterial spin labeling study. Braz J Med Biol Res 2017;50(4):e5670. https://doi.org/10.1590/1414-431X20175670.

[31] Webster M. FUGUE/GUIDE. FSL - FslWiki. Accessed December 3, 2021, https://fsl.fmrib.ox.ac.uk/fsl/fslwiki/FUGUE/Guide; 2021.

[32] Bause J, Polimeni JR, Stelzer J, et al. Impact of prospective motion correction, distortion correction methods and large vein bias on the spatial accuracy of cortical laminar fMRI at 9.4 tesla. NeuroImage. 2020;208:116434. https://doi.org/10.1016/j.neuroimage.2019.116434.

[33] Renvall V, Witzel T, Wald LL, Polimeni JR. Automatic cortical surface reconstruction of high-resolution T1 echo planar imaging data. NeuroImage. 2016;134:338–54. https://doi.org/10.1016/j.neuroimage.2016.04.004.

[34] Groves AR, Chappell MA, Woolrich MW. Combined spatial and non-spatial prior for inference on MRI time-series. NeuroImage. 2009;45(3):795–809. https://doi.org/10.1016/j.neuroimage.2008.12.027.

[35] Chappell MA, Groves AR, MacIntosh BJ, Donahue MJ, Jezzard P, Woolrich MW. Partial volume correction of multiple inversion time arterial spin labeling MRI data. Magn Reson Med 2011;65(4):1173–83. https://doi.org/10.1002/mrm.22641.

[36] Zhang Y, Brady M, Smith S. Segmentation of brain MR images through a hidden Markov random field model and the expectation-maximization algorithm. IEEE Trans Med Imaging 2001;20(1):45–57. https://doi.org/10.1109/42.906424.

[37] Patenaude B, Smith SM, Kennedy DN, Jenkinson M. A Bayesian model of shape and appearance for subcortical brain segmentation. NeuroImage. 2011;56(3):907–22. https://doi.org/10.1016/j.neuroimage.2011.02.046.

[38] Andersson JLR, Jenkinson M, Smith S. Non-linear registration, aka spatial normalisation. In: FMRIB Technical Report TR07JA2; 2010.

[39] Mazziotta J, Toga A, Evans A, et al. A probabilistic atlas and reference system for the human brain: international consortium for brain mapping (ICBM). Philos Trans R Soc Lond B Biol Sci 2001;356(1412):1293–322. https://doi.org/10.1098/rstb.2001.0915.

[40] Martin SZ, Madai VI, von Samson-Himmelstjerna FC, et al. 3D GRASE pulsed arterial spin labeling at multiple inflow times in patients with long arterial transit times: comparison with dynamic susceptibility-weighted contrast-enhanced MRI at 3Tesla. J Cereb Blood Flow Metab 2015;35(3):392–401. https://doi.org/10.1038/jcbfm.2014.

[41] Feinberg DA, Beckett A, Chen L. Arterial spin labeling with simultaneous multi-slice echo planar imaging. Magn Reson Med 2013;70(6):1500–6. https://doi.org/10.1002/mrm.24994.

[42] Dymerska B, Poser BA, Barth M, Trattnig S, Robinson SD. A method for the dynamic correction of B0-related distortions in single-echo EPI at 7T. NeuroImage. 2018;168:321–31. https://doi.org/10.1016/j.neuroimage.2016.07.009.

[43] Chappell MA, McConnell FAK, Golay X, et al. Partial volume correction in arterial spin labeling perfusion MRI: a method to disentangle anatomy from physiology or an analysis step too far? NeuroImage. 2021;238:118236. https://doi.org/10.1016/j.neuroimage.2021.118236.

[44] Maral H, Ertekin E, Tunçyürek Ö, Özsunar Y. Effects of susceptibility artifacts on perfusion MRI in patients with primary brain tumor: a comparison of arterial spin-labeling versus DSC. AJNR Am J Neuroradiol 2020;41(2):255–61. https://doi.org/10.3174/ajnr.A6384.

[45] Zhao C, Shao X, Shou Q, et al. Whole-cerebrum distortion-free three-dimensional pseudo-continuous arterial spin labeling at 7T. medRxiv [Preprint] 2023;(25). https://doi.org/10.1101/2023.04.24.23289051.

[46] Pinto J, Chappell MA, Okell TW, et al. Calibration of arterial spin labeling data-potential pitfalls in post-processing. Magn Reson Med 2020;83(4):1222–34. https://doi.org/10.1002/mrm.28000.